Journal of Thermal Analysis and Calorimetry
https://doi.org/10.1007/s10973-020-10003-7

Mixed convection–radiation in lid-driven cavities with nanofluids and time-dependent heat-generating body

Elena V. Shulepova[1] · Mikhail A. Sheremet[1,2] · Hakan F. Oztop[3,4] · Nidal Abu-Hamdeh[4]

Received: 17 April 2020 / Accepted: 27 June 2020

Abstract
The cooling process of electronic devices having heat-generating elements is a major challenge allowing to develop electronics industry. Therefore, a creation of novel cooling techniques is an important task that can be solved numerically taking into account the multiparametric character of this problem. The mixed convection heat transfer combined with thermal radiation in a lid-driven cavity filled with an alumina–water nanofluid under the effect of sinusoidal time-dependent heat-generating solid element is studied numerically. The partial differential equations formulated in stream function–vorticity variables are solved by the finite difference method. Effects of the Rayleigh number, Reynolds number, thermal radiation parameter, heater location, volumetric heat flux oscillation frequency and nanoparticles volume fraction on liquid flow and heat transfer are analyzed. It has been found that an addition of nanoparticles leads to reduction of the heater temperature, while convective flow rate decreases also.

Keywords Mixed convection · Nanofluid · Unsteady heat-generating source · Lid-driven cavity · Finite difference method

Introduction

Nowadays, many experimental and numerical papers on convective heat transfer within enclosures with local heaters were published [1–14]. Some of them are devoted to analysis of isothermal heater effect neglecting the heater sizes [1–8], while other papers deal with heaters of finite sizes [1, 2, 9–14]. Thus, Karataş and Derbentli [15] investigated the natural convection and radiation in rectangular closed spaces with different aspect ratios. They performed also experiments on heat transfer. The variations of the temperature profile and the local Nusselt number along the cavity height are presented. Sun et al. [16] investigated the performance of the DOM, FVM, P1, SP3 and P3 methods for 2D combined natural convection and radiation heat transfer for an absorbing, emitting medium. They obtained temperature distributions, heat transfer rate and computational performance in terms of accuracy and computing time. Mahfooz et al. [17] considered the radiation effects on a transient two-dimensional natural convection for electrically conducting and optically dense fluid along a vertical flat surface in the presence of heat generation. Hashemi et al. [18] concerned with the natural convection in a porous closed space occupied by Cu–water micropolar nanofluid. They applied the Darcy model to simulate macroscopic flow dynamics in the presence of internal heating. They found that an increment in *Da* number leads to a decrease in the strength of fluid flow and microrotation of particles. Hussain et al. [19] performed a computational analysis on mixed convection in a double-sided lid-driven closed space in the presence of volumetric heat generation or absorption. They solved the governing parameters via Galerkin weighted residual finite element method in space and the Crank–Nicolson in time. They observed that heat transfer increases with increase in nanoparticle volume fraction. Dogonchi and Ganji [20] made the simultaneous of convection–radiation through a moving fin under the heat generation. In their work, the heat transfer coefficient, thermal conductivity and heat generation are varied with

✉ Mikhail A. Sheremet
Michael-sher@yandex.ru

[1] Department of Theoretical Mechanics, Tomsk State University, Tomsk, Russia 634050

[2] Laboratory on Convective Heat and Mass Transfer, Tomsk State University, Tomsk, Russia 634050

[3] Department of Mechanical Engineering, Technology Faculty, Fırat University, Elazig, Turkey

[4] Department of Mechanical Engineering, King Abdulaziz University, Jeddah, Saudi Arabia

Published online: 13 July 2020

temperature by using differential transformation method (DTM).

Karbasifar et al. [21] solved the problem of mixed convection in a lid-driven closed space with hot elliptical centric cylinder filled with nanofluid. Increase in the temperature difference between the cold walls and the cylinder at a constant Richardson number, volume fraction and cavity angle increases the Nusselt number and heat transfer in such a way that the increasing trend of the Nusselt number depends on volume fraction, fluid velocity and cavity angle. Hussain et al. [22] made serial numerical simulations to examine the effect of inclination angle on the heat transfer of nanofluid for mixed convection flows in a partially heated double lid-driven inclined closed space. At the lower wall of the closed space, two heat sources are fixed. Ahmed and Elshehabey [23] studied the buoyancy-driven heat transfer of nanofluids in inclined closed spaces in the presence of heat generation or absorption effect. In their case, the bottom and top walls of the closed space are taken as adiabatic. They found that a closed space with a square obstacle enhances the heat transfer rate with a higher rate comparing with the circular cylinder case. Raisi [24] performed a numerical analysis for the conjugate heat transfer in a square closed space filled with a copper–water nanofluid. The closed space contains a heat-generating solid square block (a heat source) at the center. Higher thermal conductivity of the heat source is related to the temperature of the nanofluid in the closed space, the temperature of the heat source and the average *Nu* number. Mansour and Ahmed [25] discussed the natural convection in an inclined triangular closed space filled with Cu–water nanofluid in the presence of porous medium and heat generation effect. They found that average Nusselt number increases with increase in the nanoparticle volume fraction and an increase in the heat generation parameter leads to a decrease in the average Nu number. Other interesting results on mixed convection in a lid-driven chamber can be found in [26–31].

Ambreen et al. [32] investigated the effects of fin shape on mixed convection heat transfer and fluid flow. Cui et al. [33] showed the effects of nanofluids on heat transfer enhancement by using field synergy analysis. Al-Kalbani and Rahman [34] investigated the convective heat transfer of nanofluid in an inclined square closed space. Control of heat transfer and fluid flow can be made by using magnetic field [35]. It has been showed that increase in power of magnetic field reduces the heat transfer. Mixed convection heat transfer and fluid flow is studied in the presence of nanofluid for vented cavities [36], double-sided lid-driven cavities with inner body [37] and lid-driven cavities [38–41] for different boundary conditions. Nanofluids are also used as control element for combustion [42]. Again, complex problems such as three-dimensional analysis in the presence of magnetic field [43] or electronical applications [44, 45] are studied. Other applications can be found in papers [46–52].

Taking into account the presented brief review, it is possible to conclude that there are no papers on mixed convection and thermal radiation in a lid-driven cavity filled with a nanofluid under the effect of the heat-conducting element with transient internal volumetric heat generation. Therefore, the aim of the present work is to study numerically mixed convection combined with thermal radiation in a square lid-driven cavity filled with an alumina–water nanofluid under the effects of transient heat-generating source. It should be noted that the present work deals with analysis of passive cooling system in the case of transient heat-generating element and thermal radiation using the smart fluid.

Basic equations

The physically mixed convective heat transfer in a square cavity with moving upper wall under the effect of local heat-generating source is depictured in Fig. 1. The domain of interest includes the square heater of size $0.2L$ with time-dependent volumetric heat generation $Q(t) = 0.5q\{1 - \sin(\xi t)\}$. This element is located on the left adiabatic side of vertical wall. The remaining walls are adiabatic too with the exception of the upper moving wall of constant low temperature T_c. This wall moves in positive x-coordinate direction with constant velocity V_0. The nanofluid contains solid spherical aluminum oxide nanoparticles, and their physical properties can be found in [53]. Thermal equilibrium between the fluid phase and nanoparticles is assumed.

It is assumed in the analysis that the nanofluid is heat-conducting, Newtonian, and the Boussinesq approximation is valid. The governing equations based on the previous assumptions in dimensional Cartesian coordinates can be written as follows:

- for the nanofluid

$$\frac{\partial \bar{u}}{\partial \bar{x}} + \frac{\partial \bar{v}}{\partial \bar{y}} = 0 \tag{1}$$

$$\rho_{\mathrm{nf}}\left(\frac{\partial \bar{u}}{\partial t} + \bar{u}\frac{\partial \bar{u}}{\partial \bar{x}} + \bar{v}\frac{\partial \bar{u}}{\partial \bar{y}}\right) = -\frac{\partial p}{\partial \bar{x}} + \mu_{\mathrm{nf}}\left(\frac{\partial^2 \bar{u}}{\partial \bar{x}^2} + \frac{\partial^2 \bar{u}}{\partial \bar{y}^2}\right) \tag{2}$$

$$\rho_{\mathrm{nf}}\left(\frac{\partial \bar{v}}{\partial t} + \bar{u}\frac{\partial \bar{v}}{\partial \bar{x}} + \bar{v}\frac{\partial \bar{v}}{\partial \bar{y}}\right) = -\frac{\partial p}{\partial \bar{y}} + \mu_{\mathrm{nf}}\left(\frac{\partial^2 \bar{v}}{\partial \bar{x}^2} + \frac{\partial^2 \bar{v}}{\partial \bar{y}^2}\right) + (\rho\beta)_{\mathrm{nf}} g\left(T - T_c\right) \tag{3}$$

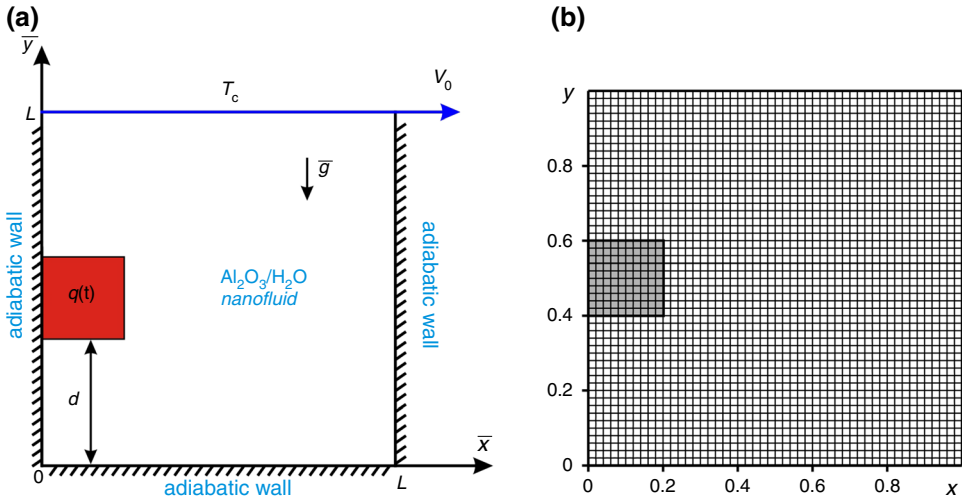

Fig. 1 Physical model (**a**) and employed uniform mesh (**b**)

$$(\rho c)_{\mathrm{nf}}\left(\frac{\partial T}{\partial t}+\bar{u}\frac{\partial T}{\partial \bar{x}}+\bar{v}\frac{\partial T}{\partial \bar{y}}\right)=k_{\mathrm{nf}}\left(\frac{\partial^2 T}{\partial \bar{x}^2}+\frac{\partial^2 T}{\partial \bar{y}^2}\right)-\left(\frac{\partial q_{\mathrm{rx}}}{\partial \bar{x}}+\frac{\partial q_{\mathrm{ry}}}{\partial \bar{y}}\right) \tag{4}$$

- for the heat-generating source

$$(\rho c)_{\mathrm{hs}}\frac{\partial T}{\partial t}=k_{\mathrm{hs}}\left(\frac{\partial^2 T}{\partial \bar{x}^2}+\frac{\partial^2 T}{\partial \bar{y}^2}\right)+Q(t) \tag{5}$$

Invoking Rosseland approximation for thermal radiation, we have [54]

$$q_{\mathrm{rx}}=-\frac{4\sigma}{3\beta_{\mathrm{r}}}\frac{\partial T^4}{\partial \bar{x}},\quad q_{\mathrm{ry}}=-\frac{4\sigma}{3\beta_{\mathrm{r}}}\frac{\partial T^4}{\partial \bar{y}} \tag{6}$$

Expanding T^4 in Taylor series about T_{c} and neglecting higher-order terms, we have $T^4\approx 4TT_{\mathrm{c}}^3-3T_{\mathrm{c}}^4$, so that we have

$$q_{\mathrm{rx}}=-\frac{16\sigma T_{\mathrm{c}}^3}{3\beta_{\mathrm{r}}}\frac{\partial T}{\partial x},\quad q_{\mathrm{ry}}=-\frac{16\sigma T_{\mathrm{c}}^3}{3\beta_{\mathrm{r}}}\frac{\partial T}{\partial y} \tag{7}$$

Introducing the stream function $\left(\bar{u}=\frac{\partial \bar{\psi}}{\partial \bar{y}},\ \bar{v}=-\frac{\partial \bar{\psi}}{\partial \bar{x}}\right)$, vorticity $\left(\bar{\omega}=\frac{\partial \bar{v}}{\partial \bar{x}}-\frac{\partial \bar{u}}{\partial \bar{y}}\right)$, and the following dimensionless variables:

$$x=\bar{x}/L,\quad y=\bar{y}/L,\quad \tau=V_0t/L,\quad \theta=\left(T-T_c\right)/\Delta T,$$
$$u=\bar{u}/V_0,\quad v=\bar{v}/V_0,\quad \psi=\bar{\psi}/\left(V_0L\right),$$
$$\omega=\bar{\omega}L/V_0,\quad \Delta T=qL^2/k_{\mathrm{hs}}$$

At the same time, effective viscosity and thermal conductivity are the functions of nanoparticles volume fraction that have been obtained by Ho et al. [55].

The governing equations of convective heat transfer in dimensionless variables stream function—vorticity become:

- for the nanofluid

$$\frac{\partial^2\psi}{\partial x^2}+\frac{\partial^2\psi}{\partial y^2}=-\omega \tag{8}$$

Table 2 Mean Nusselt number at the hot border for Ra = 8.663×10^7 and Pr = 7.002

Alumina nanoparticles volume fraction	0.01	0.02	0.03
Experimental results [55]	32.2037	31.0905	29.0769
Obtained numerical data	31.6043	31.2538	30.829

Table 1 Mean Nusselt number at the moving border for Gr = 100 and Pr = 0.71

Reference	Re				
	1	100	400	500	1000
Data of Abu-Nada and Chamkha [56]	1.010134	2.090837	4.162057	4.663689	6.551615
Data of Waheed [57]	1.00033	2.03116	4.02462	4.52671	6.48423
Obtained data	1.00033	2.04935	4.09826	4.6179	6.70345

$$\frac{\partial \omega}{\partial \tau} + u\frac{\partial \omega}{\partial x} + v\frac{\partial \omega}{\partial y} = \frac{H_1(\phi)}{\mathrm{Re}}\left(\frac{\partial^2 \omega}{\partial x^2} + \frac{\partial^2 \omega}{\partial y^2}\right) + H_2(\phi)\frac{\mathrm{Ra}}{\mathrm{Pr}\cdot \mathrm{Re}^2}\frac{\partial \theta}{\partial x} \tag{9}$$

$$\frac{\partial \theta}{\partial \tau} + u\frac{\partial \theta}{\partial x} + v\frac{\partial \theta}{\partial y} = \frac{H_3(\phi)}{\mathrm{Re}\cdot \mathrm{Pr}}\left(\frac{\partial^2 \theta}{\partial x^2} + \frac{\partial^2 \theta}{\partial y^2}\right) \tag{10}$$

- for the heat-generating element

$$\frac{\partial \theta}{\partial \tau} = \frac{\alpha_{\mathrm{hs}}/\alpha_{\mathrm{f}}}{\mathrm{Re}\cdot \mathrm{Pr}}\left(\frac{\partial^2 \theta}{\partial x^2} + \frac{\partial^2 \theta}{\partial y^2} + \frac{1}{2}\{1-\sin(f\tau)\}\right) \tag{11}$$

The initial and boundary conditions for the formulated problem (6)–(9) are as follows:

$$\begin{aligned}
&\tau = 0: \ \psi = \omega = \theta = 0 \quad \text{at} \quad 0 \le x \le 1 \ \text{and} \ 0 \le y \le 1\\
&\tau > 0: \ \psi = 0, \ \frac{\partial \psi}{\partial x} = 0, \ \omega = -\frac{\partial^2 \psi}{\partial x^2}, \ \frac{\partial \theta}{\partial x} = 0 \quad \text{at } x = 0, \quad 1 \ \text{and} \ 0 \le y \le 1\\
&\qquad \psi = 0, \ \frac{\partial \psi}{\partial y} = 0, \ \omega = -\frac{\partial^2 \psi}{\partial y^2}, \ \frac{\partial \theta}{\partial y} = 0 \quad \text{at } y = 0 \ \text{and} \ 0 < x < 1\\
&\qquad \psi = 0, \ \frac{\partial \psi}{\partial y} = 1, \ \omega = -\frac{\partial^2 \psi}{\partial y^2}, \ \theta = 0 \ \text{at } y = 1 \ \text{and} \ 0 < x < 1\\
&\qquad \psi = 0, \ \omega = -\frac{\partial^2 \psi}{\partial n^2}, \ \begin{cases} \theta_{\mathrm{hs}} = \theta_{\mathrm{nf}} \\ \frac{\partial \theta_{\mathrm{hs}}}{\partial n} = H_4(\phi)\frac{\partial \theta_{\mathrm{nf}}}{\partial n} \end{cases} \quad \text{at heat source surface}
\end{aligned} \tag{12}$$

Here, Re is the Reynolds number; Ra is the Rayleigh number; Pr is the Prandtl number; R_{d} is the radiation parameter, f is the dimensionless oscillation frequency and there are the additional functions $H_1(\phi)$, $H_2(\phi)$, $H_3(\phi)$ and $H_4(\phi)$, which are defined as

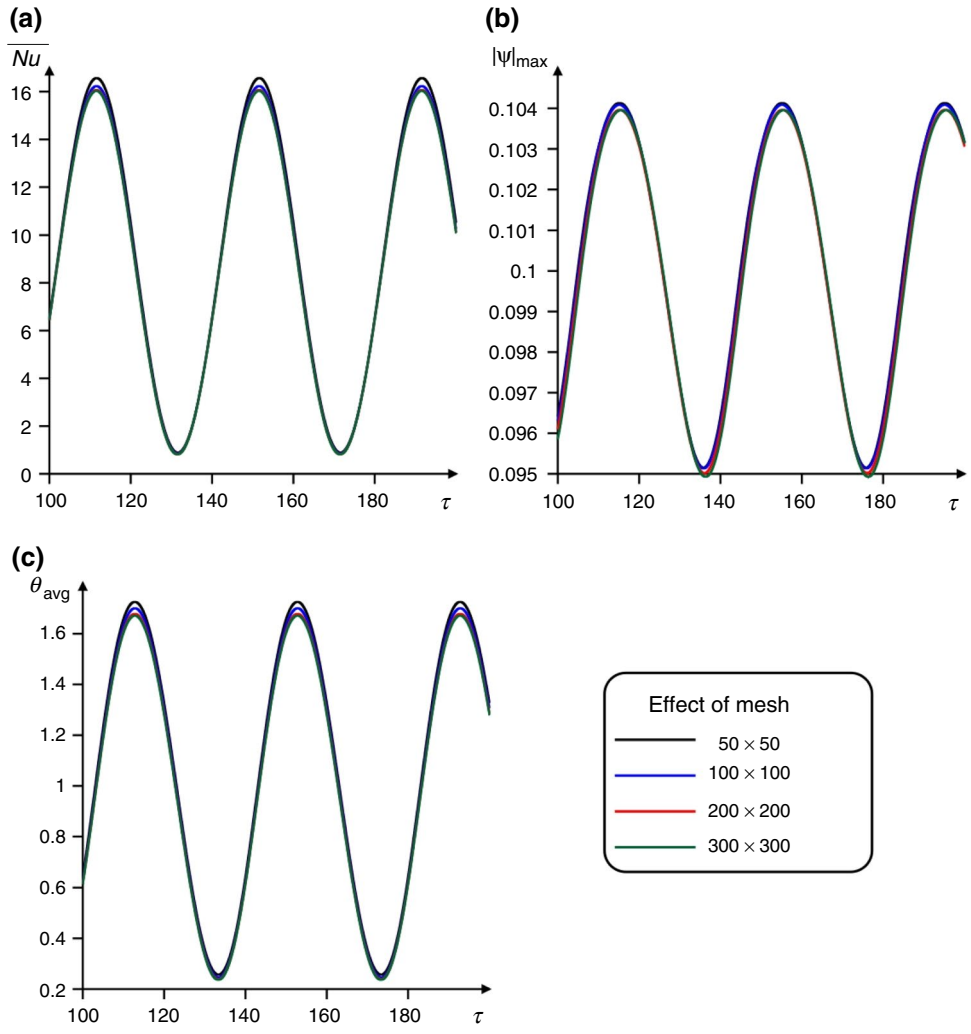

Fig. 2 Variation of the average Nusselt number (**a**), maximum absolute value of the stream function (**b**) and average temperature inside the heater (*i*) versus the dimensionless time and the mesh parameters

$$\mathrm{Re}=\frac{\rho V_0 L}{\mu},\quad \mathrm{Ra}=\frac{\rho g\beta\Delta T L^3}{\alpha\mu},\quad \mathrm{Pr}=\frac{\mu}{\rho\alpha},\quad R_\mathrm{d}=\frac{4\sigma T_\mathrm{c}^3}{k_\mathrm{f}\beta_\mathrm{r}},f=\frac{\xi L}{V_0},\quad H_1(\phi)=\frac{1+4.93\phi+222.4\phi^2}{1-\phi+\phi\rho_\mathrm{p}/\rho_\mathrm{f}},$$
$$H_2(\phi)=\frac{1-\phi+\phi(\rho\beta)_\mathrm{p}/(\rho\beta)_\mathrm{f}}{1-\phi+\phi\rho_\mathrm{p}/\rho_\mathrm{f}},\quad H_3(\phi)=\frac{1+2.944\phi+19.672\phi^2}{1-\phi+\phi(\rho c)_\mathrm{p}/(\rho c)_\mathrm{f}}\left[1+\frac{4R_\mathrm{d}}{3\left(1+2.944\phi+19.672\phi^2\right)}\right], \tag{13}$$
$$H_4(\phi)=\frac{1+2.944\phi+19.672\phi^2}{k_\mathrm{hs}/k_\mathrm{f}}$$

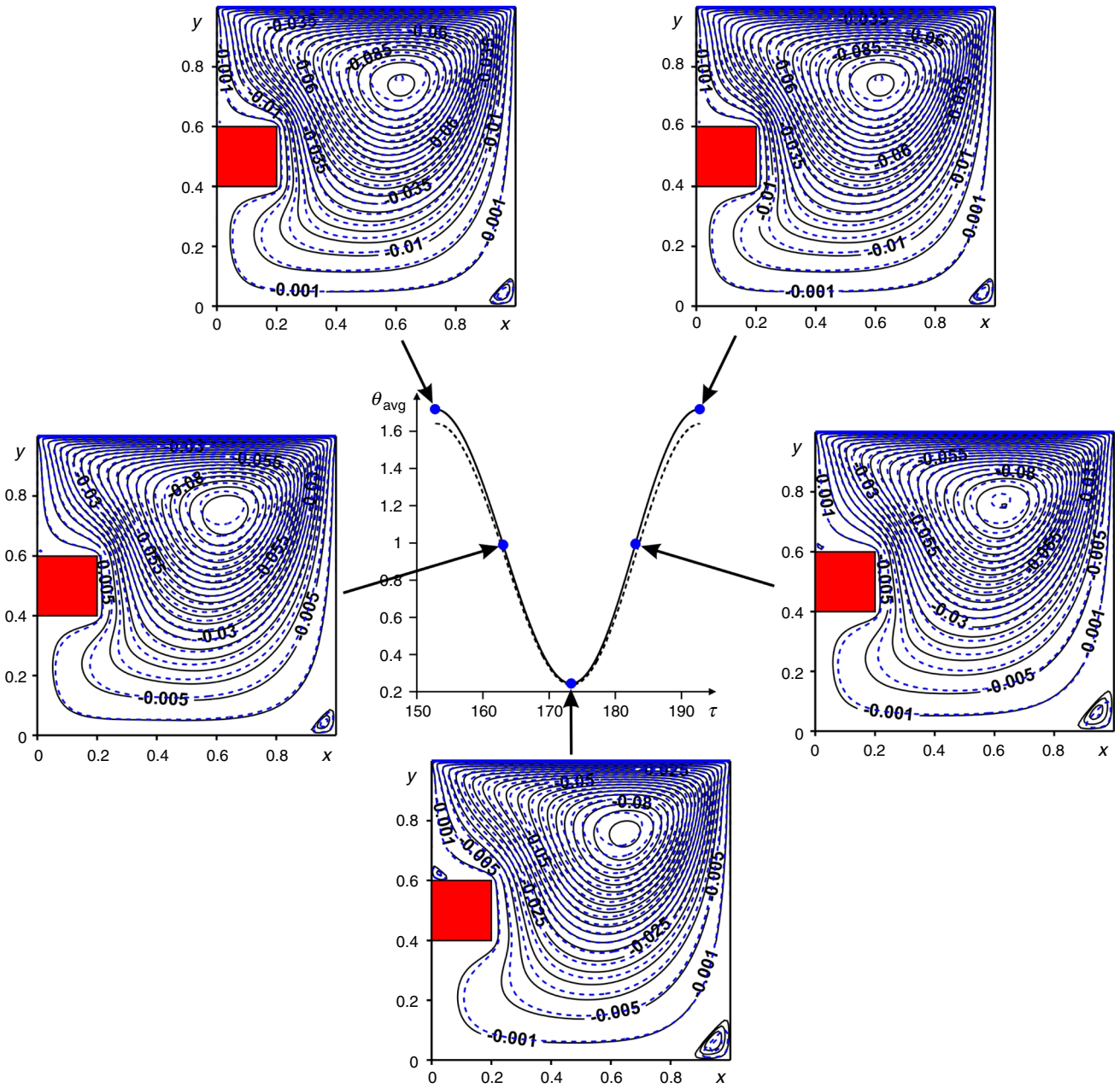

Fig. 3 Evolution of streamlines for $\mathrm{Ra}=10^5$, $\mathrm{Re}=100$, $R_\mathrm{d}=1$, $\delta=0.4$, $f=0.05\pi$ at $\phi=0.0$ (solid lines) and $\phi=0.04$ (dashed lines)

The physical quantity of interest is the average Nusselt number at heat source surface defined as:

$$\overline{Nu} = \frac{1}{l}\int_0^l \left(-\frac{k_{nf}}{k_f}\frac{\partial\theta}{\partial n}\right)\mathrm{d}\zeta \tag{14}$$

Here, the effective thermal conductivity of the nanofluid was defined using the empirical data of Ho et al. [55] as follows: $k_{nf} = k_f\left(1 + 2.944\phi + 19.672\phi^2\right)$.

Numerical method

The partial differential Eqs. (8)–(11) with corresponding initial and boundary conditions (12) have been solved by finite difference method using the uniform grid [10–12, 53, 54]. The complicated validation analysis has been performed earlier [10–12, 53, 54].

In the case of a convective energy transport in a lid-driven chamber, the developed computational code has

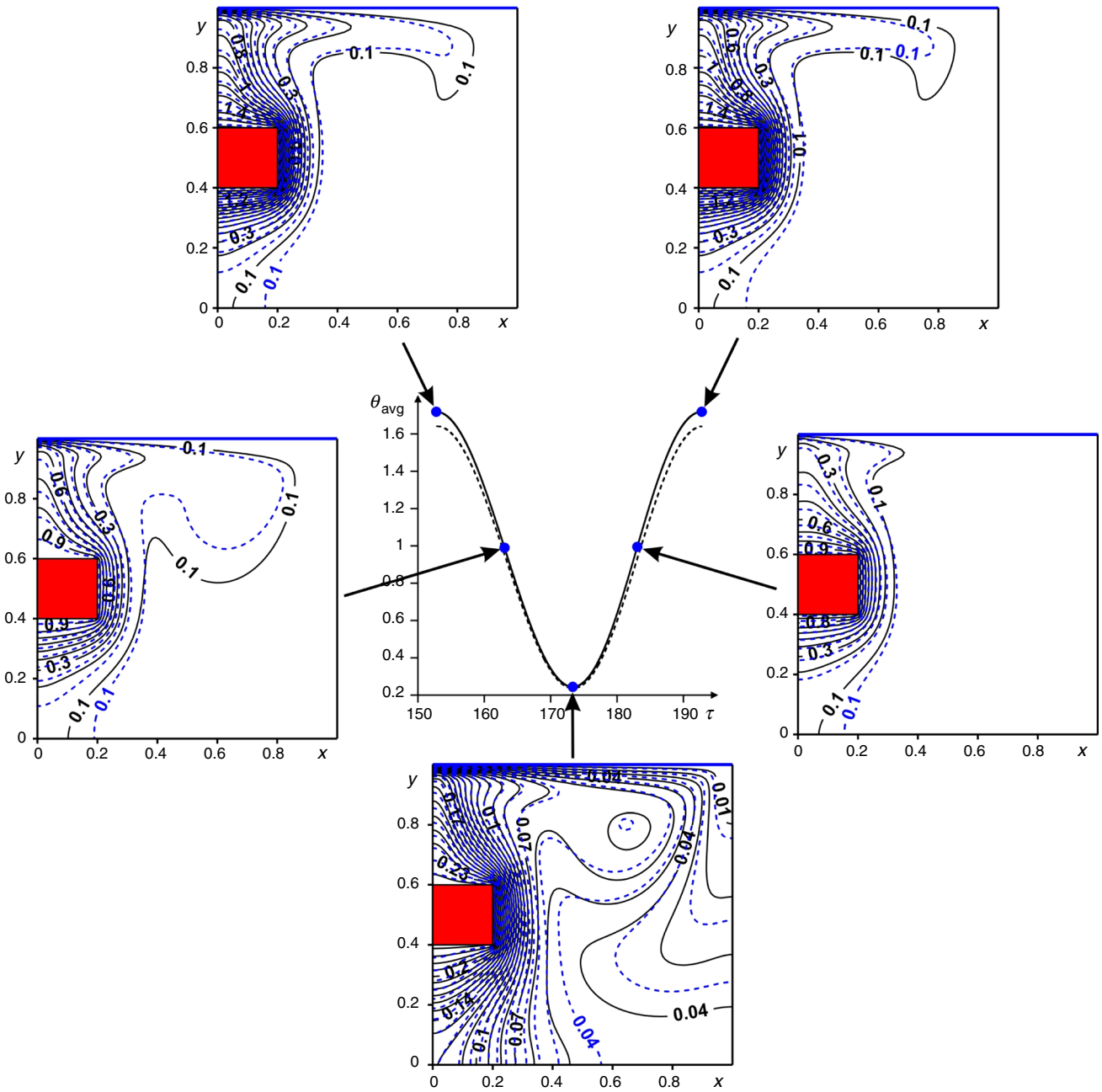

Fig. 4 Evolution of isotherms for Ra = 10^5, Re = 100, $R_d = 1$, $\delta = 0.4$, $f = 0.05\pi$ at $\phi = 0.0$ (solid lines) and $\phi = 0.04$ (dashed lines)

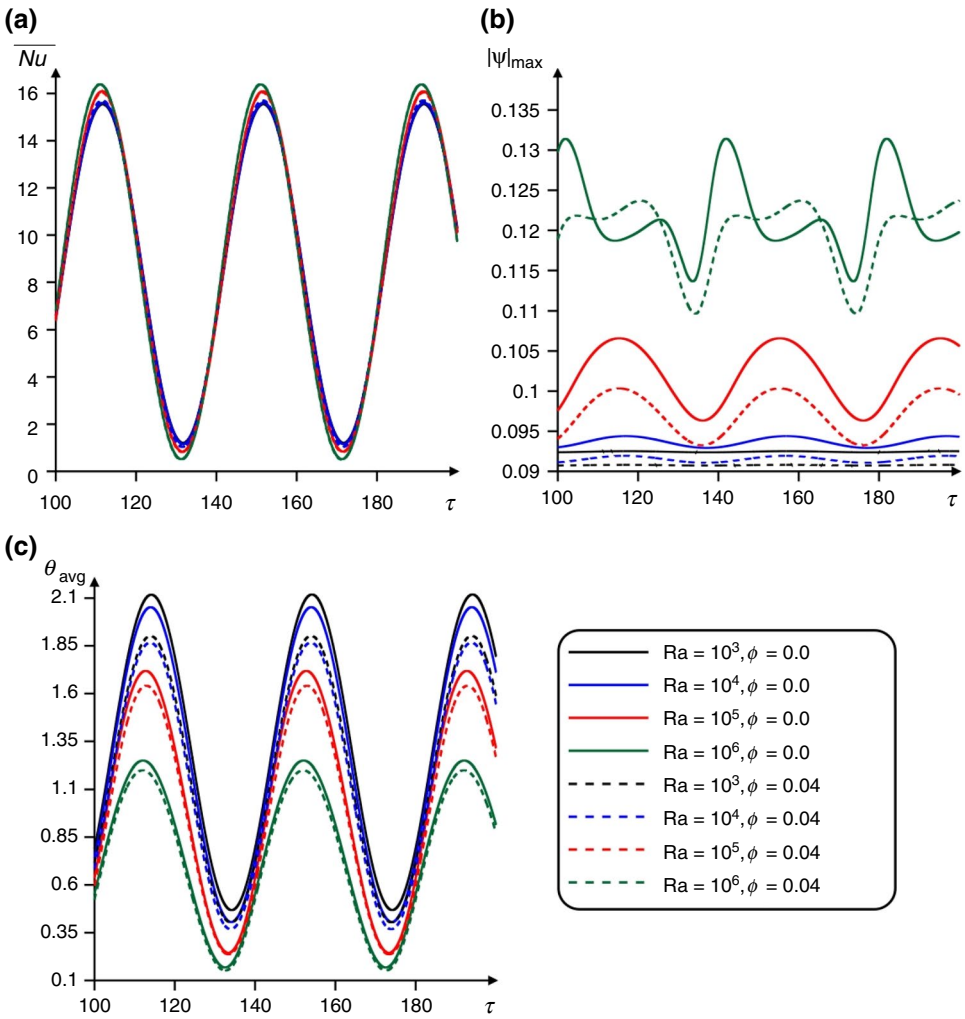

Fig. 5 Variation of mean Nusselt number $\left(\overline{Nu}\right)$ (**a**), liquid motion rate (**b**) and average temperature inside the heater (*c*) with the dimensionless time for Re = 100, $R_d = 1$, $\delta = 0.4$, $f = 0.05\pi$, different values of Rayleigh number and nanoparticles volume fraction

been verified using the numerical data of [56, 57]. Table 1 demonstrates a very good comparison for the mean Nusselt number at the moving top border for Gr = 100 and Pr = 0.71.

In the case of alumina–water nanosuspended natural convection within a square region, the developed code has been verified using the experimental data of Ho et al. [55]. Table 2 shows a very good agreement with experimental data for the mean Nusselt number at heated border.

The method of solution has been tested on different meshes. Figure 2 shows the sensitivity of the average Nusselt number at the heater surface, maximum absolute value of the stream function and average temperature inside the heater for Re = 100, $Ra = 10^5$, Pr = 6.82, $R_d = 1$, $\phi = 0.02$, $\delta = d/L = 0.4$, $f = 0.05\pi$.

Taking into account the obtained results for $0 \le \tau \le 200$, the computational mesh of 200 × 200 has been selected for an investigation owing to obtain an appropriate accuracy and optimal calculation time. A sample of the used uniform mesh is presented in Fig. 1*b*.

Results and discussion

A numerical study has been conducted for the following values of the control parameters as: Rayleigh number ($Ra = 10^3$–10^6), Reynolds number (Re = 50–500), Prandtl number (Pr = 6.82), radiation parameter ($R_d = 0$–3), nanoparticles volume fraction ($0 \le \phi \le 0.04$), heat source location ($0.1 \le \delta \le 0.7$), volumetric heat flux oscillation frequency ($f = 0.01\pi$–0.1π) and heat source material (silicon). The used thermal properties of the alumina/water nanofluid and heat source material can be found in [53, 58]. Particular efforts have been focused on the effects of these parameters on the fluid flow and heat transfer. Streamlines, isotherms, average Nusselt numbers at the heater surface, nanofluid flow rate and average temperature inside the heater for different values of governing parameters mentioned above are illustrated in Figs. 3–9.

Figure 3 shows the streamlines during one period for the heater average temperature at $Ra = 10^5$, Re = 100, $R_d = 1$,

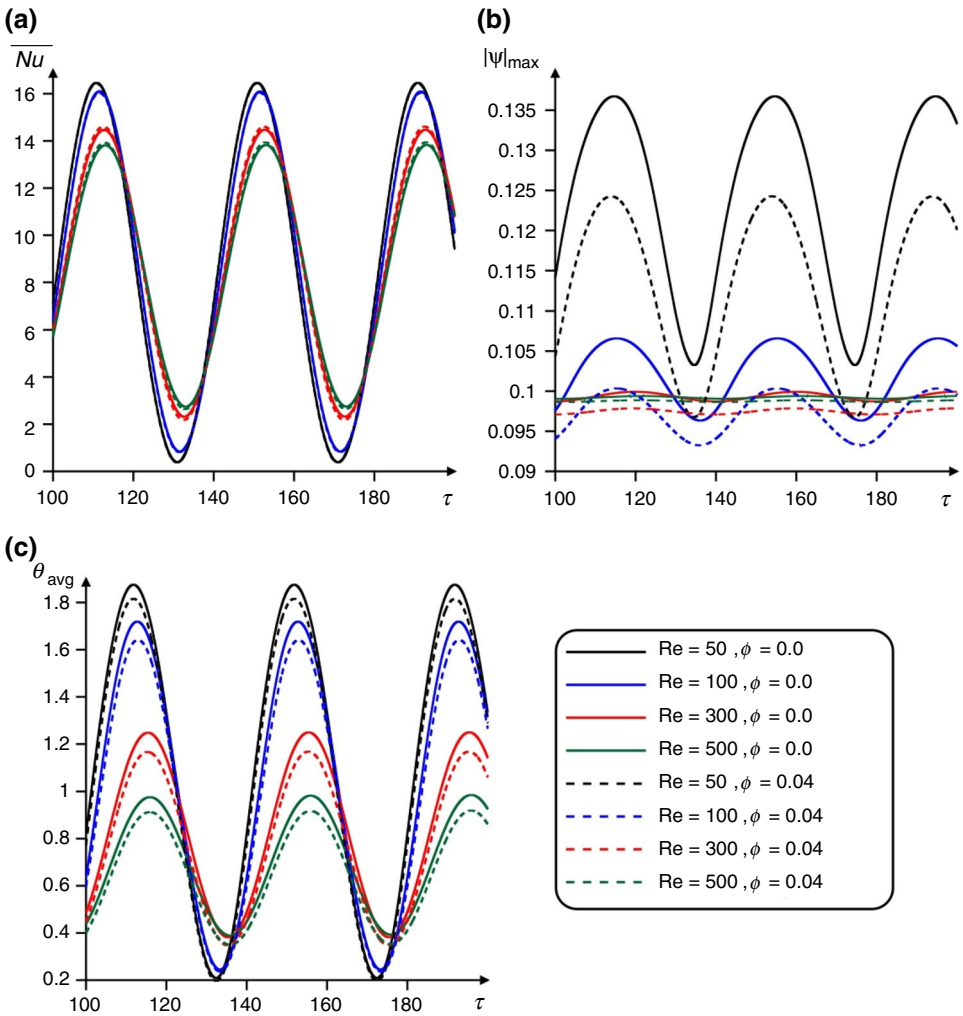

Fig. 6 Variation of mean Nusselt number $\left(\overline{Nu}\right)$ (**a**), liquid motion rate (**b**) and average temperature inside the heater (*c*) with the dimensionless time for $\mathrm{Ra}=10^5$, $R_\mathrm{d}=1$, $\delta=0.4$, $f=0.05\pi$, different values of Reynolds number and nanoparticles volume fraction

$\delta=0.4$, $f=0.05\pi$ and different values of nanoparticles concentration. Regardless of the considered dimensionless time values at quasi-stationary mode, one clockwise convective circulation is formed inside the cavity reflecting an ascending flows near the heater and descending flows near the right vertical wall. Such flow nature can be explained by the heater location and the effect of the moving upper wall. The flow structures for all considered time values are typical, and they do not have any essential differences. Some differences can be found in the size of the right bottom corner recirculation. Namely, a growth of this recirculation scale can be found for low heater temperature and during the next several time points when this temperature rises. Moreover, an additional recirculation places over the heated element and the size of this vortex has the similar behavior. Also, it is possible to conclude that in the case of low θ_avg the fluid flow rate is low also. An insertion of nanoparticles leads to a growth of the liquid viscosity and as a result, convective flow intensity reduces. At the same time, the heater average temperature decreases also due to a rise of the liquid effective thermal conductivity. It is interesting to note that maximum values of θ_avg are reduced, while the minimum value changes weakly. Such behavior can be explained by low impact of the internal volumetric heat generation for this time moment. It should be noted that in the case of nanofluid ($\phi=0.04$) the size of right bottom corner minor vortex is less than for pure fluid ($\phi=0.0$).

Distributions of the isotherms are presented in Fig. 4 to illustrate different style of the thermal plume formation over the heater. Taking into account the formed flow structures inside the cavity, thermal plume develops along the left vertical wall, while heating of the right and bottom parts occurs due to heat conduction. In the case of high average

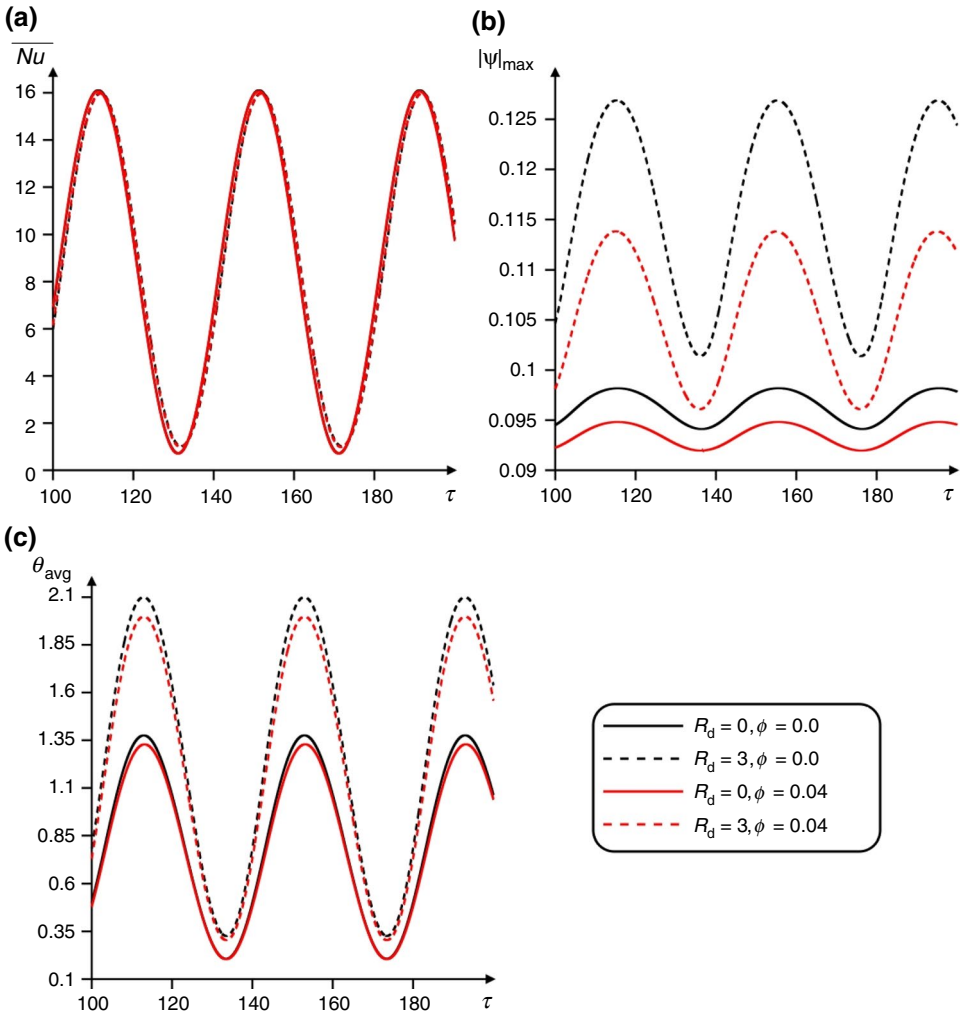

Fig. 7 Variation of mean Nusselt number $\left(\overline{Nu}\right)$ (**a**), liquid motion rate (**b**) and average temperature inside the heater (*c*) with the dimensionless time for $Ra = 10^5$, $Re = 100$, $\delta = 0.4$, $f = 0.05\pi$, different values of radiation parameter and nanoparticles volume fraction

temperature inside the heater, when we have maximum value of the internal volumetric heat generation, isotherms near the heater have high values and isotherm $\theta = 0.1$ locates along the upper cold moving wall. As a result, upper moving wall cools the cavity. In the case of minimum θ_{avg} when internal volumetric heat flux is zero, we have low temperatures close to the heater surface and inside the heater. Such quick temperature variation inside the heater occurs due to high thermal conductivity of the heater material (silicon).

It is worth noting that an addition of nanoparticles leads to more intensive cooling of the upper part due to low dynamic viscosity and high thermal conductivity. At the same time, the bottom part is cooled not so essential like for the case of pure fluid ($\phi = 0.0$). Low internal heat flux for $\tau = 173.3$ reflects a domination of heat conduction with weak forced convective flows along the right vertical wall from the moving upper wall. Moreover, an evolution of the thermal plume over the heater illustrates the inertia of the working fluid. Namely, when the average heater temperature decreases one can find a formation of stable thermal plume over the heater, while for a growth of the average heater temperature this thermal plume distorts. Such changes can be found in comparison between $\tau = 163.05$ and $\tau = 183.05$. For these time points $\theta_{avg} = 1.0$, but the temperature fields are differ due to a finite temperature distribution rate.

Figure 5 characterizes the influence of dimensionless time, Rayleigh number and nanoparticles volume fraction on the average Nusselt number along the heater surface, liquid flow rate inside the cavity and average temperature within the heater. The considered time moments reflect a formation of periodic quasi-stationary mode. Increase in the Rayleigh number results in a weak increase in the average Nusselt number and fluid flow rate, while average temperature inside the heater decreases with Ra due to more intensive circulation. It is well known that high values of the Rayleigh number illustrate more intensive convective flow.

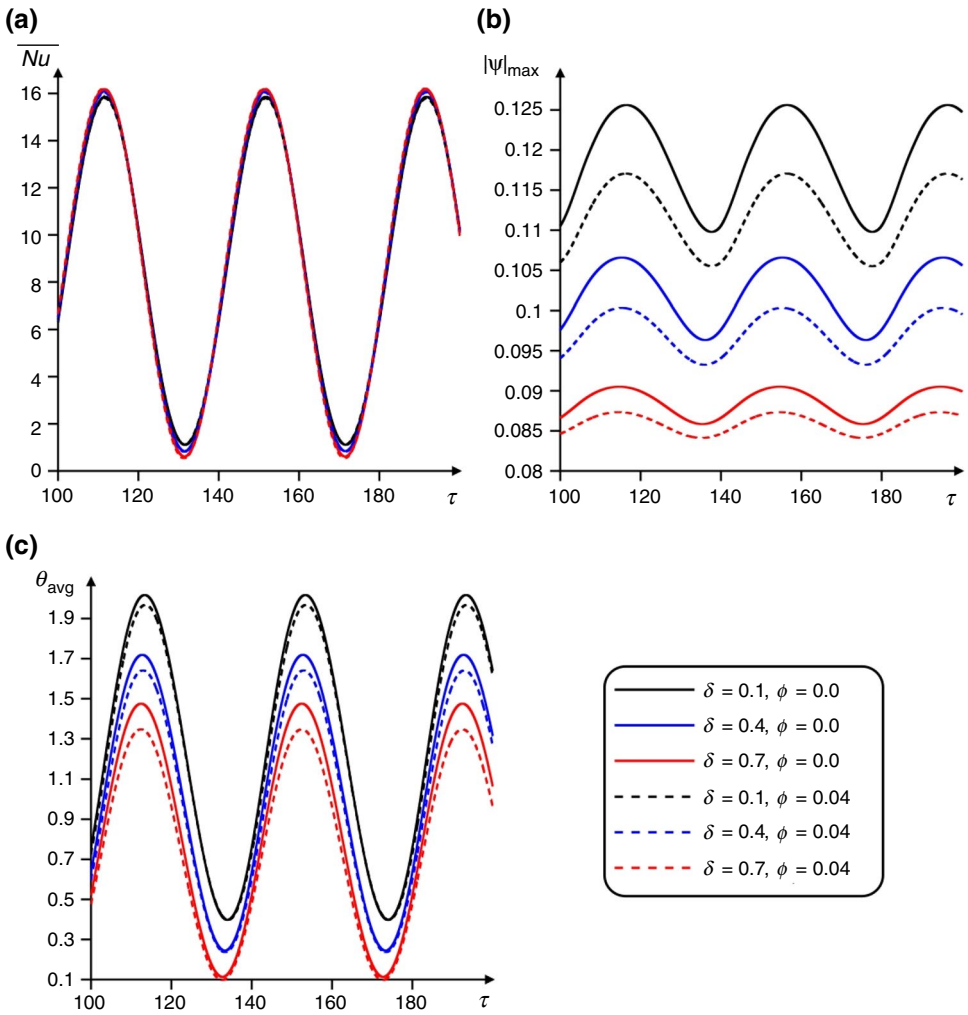

Fig. 8 Variation of mean Nusselt number $\left(\overline{Nu}\right)$ (**a**), liquid motion rate (**b**) and average temperature inside the heater (**c**) with the dimensionless time for $Ra = 10^5$, $Re = 100$, $R_d = 1$, $f = 0.05\pi$, different values of heater location and nanoparticles volume fraction

Liquid flow rate reflects also low-intensive circulation inside the enclosure for low values of the Rayleigh number, when heat conduction is a dominated heat transfer mechanism. $|\Psi|_{max}$ increases with Ra. Complicated changing of $|\Psi|_{max}$ for $Ra = 10^6$ characterizes the significant intensification of convective flow and a formation of chaotic flow nature, but the regime is still periodic. Such complicated shape of this profile illustrates more complex flow modification compared to the heat transfer performance that reflects a dependence of the flow structure on buoyancy force compared to energy transport performance.

At the same time, an addition of nanoparticles leads to weak growth of $\overline{Nu}$, while $|\Psi|_{max}$ decreases and θ_{avg} decreases also with ϕ. The latter is more desirable behavior taking into account the objective of the passive cooling system. At the same time, more intensive cooling of the heat-generating element with nanoparticles occurs for low values of the Rayleigh number, where heat conduction is a dominate heat transfer regime. Such result was mentioned in some published papers [59, 60] that characterize more essential influence of the nanoparticles only for the heat conduction regimes.

An impact of the Reynolds number combined with nanoparticles volume fraction and dimensionless time is presented in Fig. 6. The effect of nanoparticles volume fraction has been described above. In the case of Re influence, one can find a reduction of all considered parameters. Therefore, a growth of the upper moving velocity leads to the cooling of the heated element. It should be noted that an increase of the Reynolds number leads to a weak displacement of the oscillation period for all considered parameters. Moreover, more intensive motion of the upper border leads to strong reduction of the oscillation amplitude for the fluid circulation rate. Therefore, the velocity of upper moving border can suppress the oscillating influence of the periodic volumetric heat generation of the heater on the fluid circulation.

The effect of the thermal radiation parameter on the considered integral characteristics is shown in Fig. 7. A growth of R_d leads to small changes of the average Nusselt number,

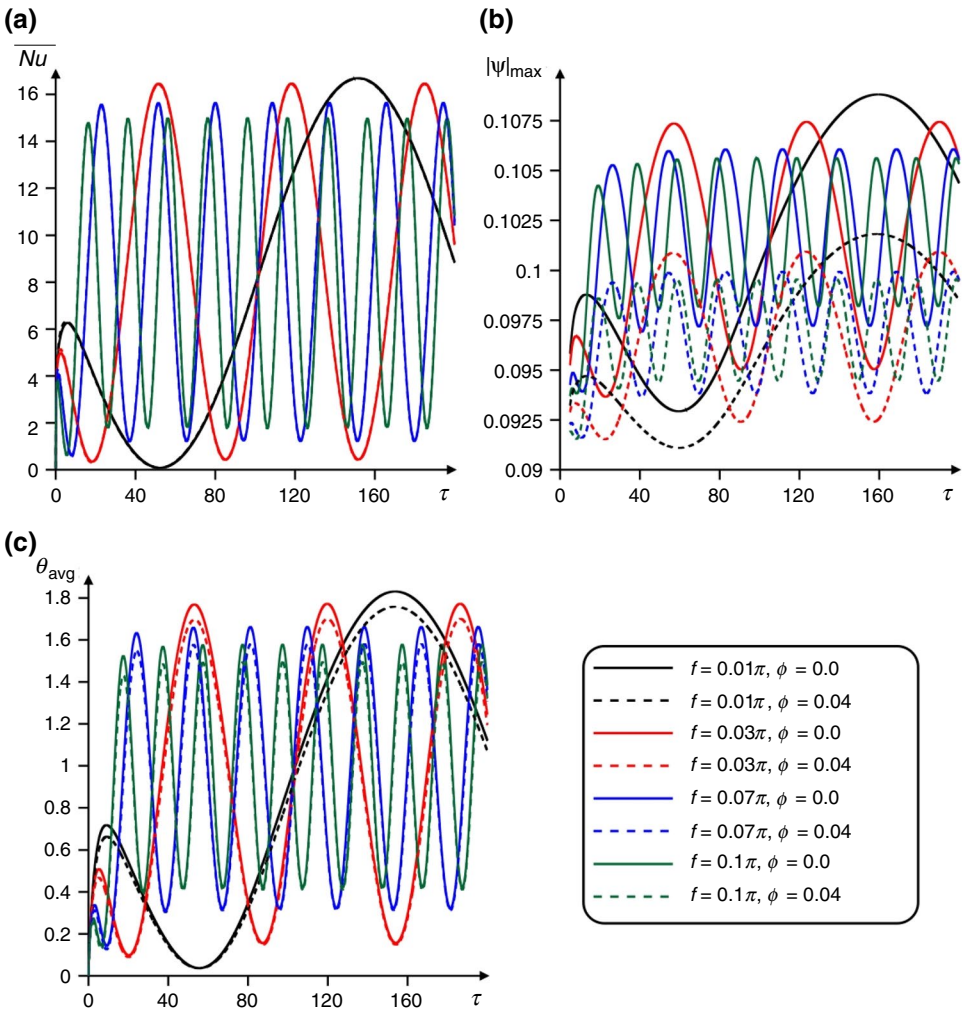

Fig. 9 Variation of mean Nusselt number $\left(\overline{Nu}\right)$ (**a**), liquid motion rate (**b**) and average temperature inside the heater (**c**) with the dimensionless time for $Ra = 10^5$, $Re = 100$, $R_d = 1$, $\delta = 0.4$, different values of volumetric heat flux oscillation frequency and nanoparticles volume fraction

while nanofluid flow rate increases with R_d and as a result the average heater temperature augments also.

It is interesting to note that the impact of the nanoparticles volume fraction is more essential for high values of the thermal radiation parameter. In the case of small changes of the average Nusselt number, it is possible to notice the complex nature of this parameter that depends not only on the fluid and solid material properties but also the formed flow and heat transfer regime.

Figure 8 demonstrates the variations of the average Nusselt number, liquid flow rate and average heater temperature with dimensionless time, the heater location and nanoparticles concentration for $Ra = 10^5$, $Re = 100$, $R_d = 1$, $f = 0.05\pi$. A displacement of the heater from the bottom wall ($\delta = 0.1$) to the upper border ($\delta = 0.7$) leads to the small variation of $\overline{Nu}$, while liquid flow rate reduces and heater average temperature diminishes also. The latter occurs due to the proximity of the cold wall to the heated element. The effect of the nanoparticles on the average heater temperature is significant when the heated element is located near the upper moving cold wall. At the same time, a displacement of the heater from the lower border till the upper one characterizes a weak displacement of the oscillation period. Such modification can be found for the average heater temperature and liquid circulation strength. It is interesting to note that the proximity of the cold border reduces the oscillation amplitude for the liquid motion strength and average heater temperature.

The impact of the volumetric heat flux oscillation frequency on $\overline{Nu}$, $|\Psi|_{max}$ and θ_{avg} is demonstrated in Fig. 9. A growth of the oscillation frequency leads to a reduction of the oscillation period for the considered control parameters. At the same time, the oscillation amplitude decreases also with f. As a result, low value of the volumetric heat flux oscillation frequency can lead to an appearance of high values of the average heater temperature that can be a reason for the system failure.

Conclusions

The mixed convection heat transfer combined with thermal radiation in a lid-driven cavity filled with an alumina–water nanofluid under the impact of the heat-generating solid element with a time-dependent internal volumetric heat flux has been studied. Governing equations formulated using the non-dimensional stream function, vorticity and temperature have been solved numerically by the finite difference method. Effects of the Rayleigh number, Reynolds number, the thermal radiation parameter, heater location, volumetric heat flux oscillation frequency and nanoparticles volume fraction on liquid flow and heat transfer have been investigated. It has been revealed that the average Nusselt number, liquid flow rate and average heater temperature are the periodic functions for the quasi-stationary regime. At the same time, the average Nusselt number is an increasing function of the Rayleigh number, thermal radiation parameter, nanoparticles volume fraction and distance between the heater and bottom wall, while $\overline{Nu}$ decreases with the Reynolds number and volumetric heat flux oscillation frequency. More important parameter for analysis of passive cooling system is an average heater temperature. It has been ascertained that an insertion of nanoparticles, a growth of the upper wall velocity, a reduction of the distance between the heater and the upper wall and a rise of the volumetric heat flux oscillation frequency can essentially reduce the heater temperature. Therefore, the alumina nanoparticles and moving cold wall can be very good control parameters for the passive cooling system.

Acknowledgements This work of Mikhail A. Sheremet was conducted as a government task of the Ministry of Science and Higher Education of the Russian Federation (Project Number 0721-2020-0036). Authors also wish to express their thanks to the very competent reviewers for their valuable comments and suggestions.

References

1. Oztop HF, Estelle P, Yan W-M, Al-Salem K, Orfi J, Mahian O. A brief review of natural convection in enclosures under localized heating with and without nanofluids. Int Commun Heat Mass Transf. 2015;60:37–44.
2. Miroshnichenko IV, Sheremet MA. Turbulent natural convection heat transfer in rectangular enclosures using experimental and numerical approaches: a review. Renew Sustain Energy Rev. 2018;82:40–59.
3. Yu Q, Xu H, Liao S. Analysis of mixed convection flow in an inclined lid-driven enclosure with Buongiorno's nanofluid model. Int J Heat Mass Transf. 2018;126:221–36.
4. Sivasankaran S, Alsabery AI, Hashim I. Internal heat generation effect on transient natural convection in a nanofluid-saturated local thermal non-equilibrium porous inclined cavity. Phys A. 2018;509:275–93.
5. Kefayati GHR, Tang H. MHD thermosolutal natural convection and entropy generation of Carreau fluid in a heated enclosure with two inner circular cold cylinders, using LBM. Int J Heat Mass Transf. 2018;126:508–30.
6. Dogonchi AS, Tayebi T, Chamkha AJ, Ganji DD. Natural convection analysis in a square enclosure with a wavy circular heater under magnetic field and nanoparticles. J Therm Anal Calorim. 2020;139:661–71.
7. Dogonchi AS, Armaghani T, Chamkha AJ, Ganji DD. Natural convection analysis in a cavity with an inclined elliptical heater subject to shape factor of nanoparticles and magnetic field. Arab J Sci Eng. 2019;44:7919–31.
8. Mansour MA, Bakeir MA, Chamkha A. Natural convection inside a C-shaped nanofluid-filled enclosure with localized heat sources. Int J Numer Meth Heat Fluid Flow. 2014;24(8):1954–78.
9. Razera AL, da Fonseca RJC, Isoldi LA, dos Santos ED, Rocha LAO, Biserni C. Constructal design of a semi-elliptical fin inserted in a lid-driven square cavity with mixed convection. Int J Heat Mass Transf. 2018;126:81–94.
10. Bondareva NS, Sheremet MA. Flow and heat transfer evolution of PCM due to natural convection melting in a square cavity with a local heater. Int J Mech Sci. 2017;134:610–9.
11. Mikhailenko SA, Sheremet MA. Convective heat transfer combined with surface radiation in a rotating square cavity with a local heater. Numer Heat Transf A. 2017;72:697–707.
12. Miroshnichenko IV, Sheremet MA, Mohamad AA. Numerical simulation of a conjugate turbulent natural convection combined with surface thermal radiation in an enclosure with a heat source. Int J Therm Sci. 2016;109:172–81.
13. Sheikholeslami M, Shehzad SA, Li Z. Water based nanofluid free convection heat transfer in a three dimensional porous cavity with hot sphere obstacle in existence of Lorenz forces. Int J Heat Mass Transf. 2018;125:375–86.
14. Mohebbi R, Izadi M, Chamkha AJ. Heat source location and natural convection in a C-shaped enclosure saturated by a nanofluid. Phys Fluids. 2017;29:122009.
15. Karatas H, Derbentli T. Natural convection and radiation in rectangular cavities with one active vertical wall. Int J Therm Sci. 2018;123:129–39.
16. Sun Y, Zhang X, Howell JR. Assessment of different radiative transfer equation solvers for combined natural convection and radiation heat transfer problems. J Quant Spectrosc Radiat Transf. 2017;194:31–46.
17. Mahfooz SM, Hossain MA, Gorla RSR. Radiation effects on transient magnetohydrodynamic natural convection flow with heat generation. Int J Therm Sci. 2012;58:79–91.
18. Hashemi H, Namazian Z, Mehryan SAM. Cu-water micropolar nanofluid natural convection within a porous enclosure with heat generation. J Mol Liq. 2017;236:48–60.
19. Hussain S, Öztop HF, Mehmood K, Abu-Hamdeh N. Effects of inclined magnetic field on mixed convection in a nanofluid filled double lid-driven cavity with volumetric heat generation or absorption using finite element method. Chin J Phys. 2018;56:484–501.
20. Dogonchi AS, Ganji DD. Convection–radiation heat transfer study of moving fin with temperature-dependent thermal conductivity, heat transfer coefficient and heat generation. Appl Therm Eng. 2016;103:705–12.
21. Karbasifar B, Akbari M, Toghraie D. Mixed convection of Water–Aluminum oxide nanofluid in an inclined lid-driven cavity containing a hot elliptical centric cylinder. Int J Heat Mass Transf. 2018;116:1237–49.
22. Hussain S, Ahmad S, Mehmood K, Sagheer M. Effects of inclination angle on mixed convective nanofluid flow in a double

lid-driven cavity with discrete heat sources. Int J Heat Mass Transf. 2017;106:847–60.
23. Ahmed SE, Elshehabey HM. Buoyancy-driven flow of nanofluids in an inclined enclosure containing an adiabatic obstacle with heat generation/absorption: effects of periodic thermal conditions. Int J Heat Mass Transf. 2018;124:58–73.
24. Raisi A. Heat transfer in an enclosure filled with a nanofluid and containing a heat-generating conductive body. Appl Therm Eng. 2017;110:469–80.
25. Mansour MA, Ahmed SE. A numerical study on natural convection in porous media-filled an inclined triangular enclosure with heat sources using nanofluid in the presence of heat generation effect. Eng Sci Technol Int J. 2015;18:485–95.
26. Chamkha AJ, Abu-Nada E. Mixed convection flow in single- and double-lid driven square cavities filled with water–Al_2O_3 nanofluid: effect of viscosity models. Eur J Mech B/Fluids. 2012;36:82–96.
27. Abu-Nada E, Chamkha AJ. Mixed convection flow of a nanofluid in a lid-driven cavity with a wavy wall. Int Commun Heat Mass Transf. 2014;57:36–47.
28. Nasrin R, Alim MA, Chamkha AJ. Modeling of mixed convective heat transfer utilizing nanofluid in a double lid-driven chamber with internal heat generation. Int J Numer Meth Heat Fluid Flow. 2014;24(1):36–57.
29. Ismael MA, Pop I, Chamkha AJ. Mixed convection in a lid-driven square cavity with partial slip. Int J Therm Sci. 2014;82:47–61.
30. Selimefendigil F, Oztop HF, Chamkha AJ. MHD mixed convection and entropy generation of nanofluid filled lid driven cavity under the influence of inclined magnetic fields imposed to its upper and lower diagonal triangular domains. J Magn Magn Mater. 2016;406:266–81.
31. Alsabery AI, Armaghani T, Chamkha AJ, Hashim I. Two-phase nanofluid model and magnetic field effects on mixed convection in a lid-driven cavity containing heated triangular wall. Alexandria Eng J. 2020;59:129–48.
32. Ambreen T, Saleem A, Par CW. Pin-fin shape-dependent heat transfer and fluid flow characteristics of water- and nanofluid-cooled micropin-fin heat sinks: square, circular and triangular fin cross-sections. Appl Therm Eng. 2019;158:113781.
33. Cui W, Mao D, Lin B, Yang J. Field synergy analysis on the mechanism of heat transfer enhancement by using nanofluids. Case Stud Therm Eng. 2019;16:100554.
34. Al-Kalbani KS, Rahman MM. Convective heat transfer in the flow of a nanofluid in an inclined square enclosure. J Eng Phys Thermophys. 2019;92:1150–70.
35. Sheikholeslami M. Magnetohydrodynamic nanofluid forced convection in a porous lid driven cubic cavity using Lattice Boltzmann method. J Mol Liq. 2017;231:555–65.
36. Selimefendigil F, Öztop HF. Effects of an inner stationary cylinder having an elastic rod-like extension on the mixed convection of CNT-water nanofluid in a three dimensional vented cavity. Int J Heat Mass Transf. 2019;137:650–68.
37. Alsabery AI, Sheremet MA, Chamkha AJ, Hashim I. Impact of nonhomogeneous nanofluid model on transient mixed convection in a double lid-driven wavy cavity involving solid circular cylinder. Int J Mech Sci. 2019;150:637–55.
38. Sheremet MA, Pop I. Mixed convection in a lid-driven square cavity filled by a nanofluid: Buongiorno's mathematical model. Appl Math Comput. 2015;266:792–808.
39. Rashad AM, Ismael MA, Chamkha AJ, Mansour MA. MHD mixed convection of localized heat source/sink in a nanofluid-filled lid-driven square cavity with partial slip. J Taiwan Instit Chem Eng. 2016;68:173–86.
40. Astanina MS, Sheremet MA, Oztop HF, Abu-Hamdeh N. Mixed convection of Al_2O_3-water nanofluid in a lid-driven cavity having two porous layers. Int J Heat Mass Transf. 2018;118:527–37.
41. Gangawane KM, Manikandan B. Mixed convection characteristics in lid-driven cavity containing heated triangular block. Chin J Chem Eng. 2017;25(10):1381–94.
42. Pourhoseini SH. Enhancement of radiation characteristics and reduction of NOx emission in natural gas flame through silver-water nanofluid injection. Energy. 2020;194:116900.
43. Ghasemi K, Siavashi M. Three-dimensional analysis of magnetohydrodynamic transverse mixed convection of nanofluid inside a lid-driven enclosure using MRT-LBM. Int J Mech Sci. 2020;165:105199.
44. Hadavand M, Yousefzadeh S, Akbari OA, Pourfattahc F, Nguyen HM, Asad A. A numerical investigation on the effects of mixed convection of Ag–water nanofluid inside a sim-circular lid-driven cavity on the temperature of an electronic silicon chip. Appl Therm Eng. 2019;162:114298.
45. Kapil M, Roy D, Sharma B, Rana SC, Pramanik S, Barman RN. A numerical study of 2-D convective heat transfer of nanofluid (Al_2O_3/H_2O) in a lid driven cavity with square cylinder at the centre. Mater Today: Proc. 2019;11:700–7.
46. Bhattacharyya S, Pal SK, Pop I. Impact of nanoparticles migration on mixed convection and entropy generation of a Al_2O_3–water nanofluid inside an inclined enclosure with wavy side wall. J Therm Anal Calorim. 2019;138:3205–21.
47. Al-Rashed AAAA, Shahsavar A, Akbari M, Toghraie D, Akbari M, Afrand M. Finite volume simulation of mixed convection in an inclined lid-driven cavity filled with nanofluids: effects of a hot elliptical centric cylinder, cavity angle and volume fraction of nanoparticles. Phys A. 2019;527:121122.
48. Sheikholeslami M, Shehzad SA, Abbasi FM, Li Z. Nanofluid flow and forced convection heat transfer due to Lorentz forces in a porous lid driven cubic enclosure with hot obstacle. Comput Methods Appl Mech Eng. 2018;338:491–505.
49. Xu HJ, Xing ZB, Wang FQ, Cheng ZM. Review on heat conduction, heat convection, thermal radiation and phase change heat transfer of nanofluids in porous media: fundamentals and applications. Chem Eng Sci. 2019;195:462–83.
50. Alsabery AI, Selimefendigil F, Hashim I, Chamkha AJ, Ghalambaz M. Fluid-structure interaction analysis of entropy generation and mixed convection inside a cavity with flexible right wall and heated rotating cylinder. Int J Heat Mass Transf. 2019;140:331–45.
51. Mehryan SAM, Vaezi M, Sheremet M, Ghalambaz M. Melting heat transfer of power-law non-Newtonian phase change nano-enhanced n-octadecane-mesoporous silica ($MPSiO_2$). Int J Heat Mass Transf. 2020;151:119385.
52. Ghalambaz M, Chamkha AJ, Wen D. Natural convective flow and heat transfer of Nano-encapsulated phase change materials (NEPCMs) in a cavity. Int J Heat Mass Transf. 2019;138:738–49.
53. Astanina MS, Riahi MK, Abu-Nada E, Sheremet MA. Magnetohydrodynamic in partially heated square cavity with variable properties: discrepancy in experimental and theoretical conductivity correlations. Int J Heat Mass Transf. 2018;116:532–48.
54. Sheremet MA, Pop I. Natural convection combined with thermal radiation in a square cavity filled with a viscoelastic fluid. Int J Numer Meth Heat Fluid Flow. 2018;28:624–40.
55. Ho CJ, Li WK, Chang YS, Lin CC. Natural convection heat transfer of alumina-water nanofluid in vertical square enclosures: an experimental study. Int J Therm Sci. 2010;49:1345–53.
56. Abu-Nada E, Chamkha AJ. Mixed convection flow in a lid-driven inclined square enclosure filled with a nanofluid. Eur J Mech B/Fluid. 2010;29:472–82.

57. Waheed MA. Mixed convective heat transfer in rectangular enclosures driven by a continuously moving horizontal plate. Int J Heat Mass Transf. 2009;52:5055–63.
58. Astanina MS, Sheremet MA, Mahabaleshwar US, Singh J. Effect of porous medium and copper heat sink on cooling of heat-generating element. Energies. 2020. https://doi.org/10.3390/en13102538.
59. Sheremet MA, Oztop HF, Gvozdyakov DV, Ali ME. Impacts of heat-conducting solid wall and heat-generating element on free convection of Al_2O_3/H_2O nanofluid in a cavity with open border. Energies. 2018. https://doi.org/10.3390/en11123434.
60. Bondarenko DS, Sheremet MA, Oztop HF, Ali ME. Natural convection of Al_2O_3/H_2O nanofluid in a cavity with a heat-generating element. Heatline Vis Int J Heat nd Mass Transf. 2019;130:564–74.